Science Arts & Métiers (SAM)

is an open access repository that collects the work of Arts et Métiers Institute of Technology researchers and makes it freely available over the web where possible.

This is an author-deposited version published in: https://sam.ensam.eu
Handle ID: .http://hdl.handle.net/10985/14456

To cite this version :

T AWANE, Jean-Michel OLIVE, Shuzo MATSUOKA, Yoko MURAKAMI, Nicolas SAINTIER - Analyses of hydrogen distribution around fatigue crack on type 304 stainless steel using secondary ion mass spectrometry - International Journal of Hydrogen Energy - Vol. 36, n°14, p.8630-8640 - 2011

Any correspondence concerning this service should be sent to the repository Administrator : scienceouverte@ensam.eu

Arts et Métiers Institute of Technology

Available at www.sciencedirect.com

ScienceDirect

journal homepage: www.elsevier.com/locate/he

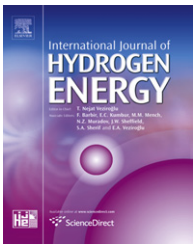

Analyses of hydrogen distribution around fatigue crack on type 304 stainless steel using secondary ion mass spectrometry

N. Saintier [a,b,c,*], T. Awane [b,c], J.M. Olive [b,c,d], S. Matsuoka [b,c], Y. Murakami [b,c]

[a] Arts et Métiers ParisTech, I2M, UMR CNRS 5295, Université de Bordeaux, Esplanade des Arts et Métiers, 33405 Talence Cedex, France
[b] Department of Mechanical Engineering, Kyushu University, Moto-oka, Nishi-ku, Fukuoka 819-0395, Japan
[c] Research Center for Hydrogen Industrial Use and Storage, National Institute of Advanced Industrial Science and Technology (HYDROGENIUS), Moto-oka, Nishi-ku, Fukuoka 819-0395, Japan
[d] CNRS, UMR 5395, I2M, Université de Bordeaux, Arts et Métiers ParisTech, Talence, France

ARTICLE INFO

Article history:
Received 3 January 2011
Received in revised form
17 March 2011
Accepted 19 March 2011
Available online 2 May 2011

Keywords:
Hydrogen
Fatigue
SIMS

ABSTRACT

Secondary Ion Mass Spectrometry (SIMS) analyses were carried out on type 304 austenitic stainless steel. On annealed specimen exposed to hydrogen (10 MPa, 358 K), Element Depth Profiles SIMS mode was able to describe quantitatively the hydrogen profile content computed by the Fick's law. Based on SIMS analyses on the wake of a fatigue crack (propagation in hydrogen gas at 0.6 MPa and RT), it was possible to compute an apparent diffusivity and solubility in the crack tip region. The apparent solubility and diffusivity in the deformed regions were two times and five orders of magnitude higher than the ones on annealed material, respectively. High hydrogen content was found around the crack tip, where the plastic deformation was well developed (pronounced slip activity). The high apparent diffusivity is presumed to result from enhanced hydrogen transport induced by cyclic plastic activity at the crack tip.

Copyright © 2011, Hydrogen Energy Publications, LLC. Published by Elsevier Ltd. All rights reserved.

1. Introduction

Hydrogen-based fuel cell systems are expected to play a major role in future solutions for carbon-rich fuel replacement and subsequent CO_2 emission reduction. From an engineering point of view, hydrogen gas transportation, storage and use in industry involve crucial issues and challenges, since hydrogen is known to interact with deformation and damage mechanisms and thus degrades material properties observed in air [1,2]. Pionneer works of Vennet et al. [3], Benson et al. [4] have highlighted the susceptibility of austenitic stainless steels to hydrogen embrittlement (HE). The effect of hydrogen on dislocation motion has been demonstrated by the experimental work of Birnbaum et al. [5]. The effect of hydrogen on the localization of strain at the micro-scale is usually believed to play a major role in the reduction of mechanical properties observed at the macro-scale [6]. Most recent works of Murakami et al. [7], Kanezaki et al. [8] have shown that, for types 316 and 304 stainless steels, hydrogen increases significantly fatigue crack growth rates. It has been observed that the effect of hydrogen on the fatigue crack growth rate was greater for steels presenting low microstructural stability such as type 304. It has been proposed that due to the higher diffusivity of hydrogen in martensite than in austenite, a significant

* *Corresponding author*. Arts et Métiers ParisTech, I2M, UMR CNRS 5295, Université de Bordeaux, Esplanade des Arts et Métiers, 33405 Talence Cedex, France.
E-mail address: nicolas.saintier@ensam.eu (N. Saintier).
0360-3199/$ – see front matter Copyright © 2011, Hydrogen Energy Publications, LLC. Published by Elsevier Ltd. All rights reserved.
doi:10.1016/j.ijhydene.2011.03.111

amount of strain-induced martensitic transformation at the crack tip acts as an hydrogen diffusion highway. Those studies highlight the effect of microstructure, local plasticity mechanisms and/or phase transformation on hydrogen distribution at the local scale. However few experimental studies deal with hydrogen content measurement at the local scale in the context of fatigue. Thermal Desorption Spectrometry (TDS) is an efficient way of evaluating the total H content within bulk specimens. For example, TDS technique has been used to estimate the apparent hydrogen solubility by using small thickness specimens and then to compute a profile of hydrogen content based on the Fick law [9]. However, it cannot allow the evaluation of hydrogen distribution at the local scale like SIMS technique. SIMS technique has been used successfully for analysing the hydrogen desorption process from ferrite, pearlite, and graphite [10]. In the context of hydrogen embrittlement studies, Tritium autoradiography and deuterium profiling by SIMS have been carried out on bolt-loaded DCB specimens of 4120 HSLA steel in order to measure the hydrogen concentration in the plastic zone at the crack tip. Though the experimental difficulties coming from the high hydrogen diffusivity in HSLA steels, a significant hydrogen enrichment at the crack tip of cathodically charged specimens could be measured [11]. In a same context, SIMS profiling of deuterated nickel-based alloy 600 have allowed to estimate a critical concentration upper limit of about 50 mass ppm for which the hydrogen-induced cracking is fully intergranular at 423 K [12].

The aim of this study is to use the SIMS technique to evaluate its ability to measure local hydrogen content in the case of stainless steels exposed to hydrogen gas environment without using deuterium and tritium. This paper presents experimental results obtained on two particular conditions. The first one concerns specimens exposed to high pressure hydrogen gas environment in order to evaluate SIMS ability to estimate known hydrogen distributions. The second one consists in hydrogen concentration evaluation around fatigue crack tips obtained after fatigue crack propagation in hydrogen gas environment. It has to be noticed that if the first case is a pure diffusion controlled process, the second case is a coupled problem where diffusion, mechanics (cyclic stress loading, cyclic plasticity, etc) and phase transformation interact. This aspects will be further discussed in the paper.

2. Experimental procedure

2.1. Material and specimens

The material used in this study is a commercial type 304 (JIS SUS304) austenitic stainless steel. Material composition is given in Table 1. Material composition was the same for all specimens considered in this study. The material has been solution heat-treated by water quenching after keeping the temperature at 1050 °C for 2 min.

Table 1 – Chemical composition (wt %, *wt ppm).

	C	Si	Mn	P	S	Ni	Cr	Mo	H*
SUS304	0.06	0.36	1.09	0.030	0.023	8.19	18.66	–	2.2

Two types of specimens have been used. For hydrogen distribution identification by SIMS, 7 mm diameter and 15 mm length cylindrical specimens were machined from round bars. Specimens have been polished using emery paper followed by final buffing with diamond paste prior to hydrogen charging (final grade 1/4 μm). For fatigue crack propagation test, standard 10 mm thick compact tension (CT) specimens have been machined from 50 mm thick plates, in the L-T direction, the middle plane of the plate corresponding to the middle plane of the specimens. The outer surface of the CT specimens has been mechanically polished using emery paper followed by final buffing with diamond paste 7 μm, 3 μm and finally using an alkaline colloidal silica suspension.

2.2. Hydrogen charging conditions and distribution

A first set of measurement was conducted to evaluate SIMS ability to quantitatively identify hydrogen distributions. For this purpose, 7 mm diameter and 15 mm length cylindrical specimens were machined from round bars made of the materials presented in Table 1 and exposed to an hydrogen pressure of 10 MPa, at 358 K, during 200 h. Such hydrogen charging conditions ensure high hydrogen concentrations at the specimen surface (above the hydrogen detection limit of SIMS) and H distributions characteristic length larger than the characteristic length of the material microstructure (in our case the grain size is about 50 μm). Moreover the expected hydrogen distribution in that case can be easily computed. It has been shown that hydrogen permeation in austenitic stainless steels exposed to gaseous hydrogen is largely controlled by diffusion which is governed by the Fick law. In the case of a semi-infinite body the analytical solution for the local hydrogen concentration is given by:

$$C_H(x,t) = C_U + (C_S - C_U) \times \left(1 - erf\left(\frac{x}{2\sqrt{Dt}}\right)\right) \quad (1)$$

where x is the distance from the surface, t is the hydrogen exposure time, D is the diffusion coefficient, C_s the hydrogen concentration at the surface and C_U is the hydrogen content in the uncharged specimen. The evolution of the diffusion coefficient of hydrogen as a function of the temperature is governed by an Arrhenius-type equation :

$$D = D_0 \exp\left(\frac{-Q}{RT}\right) \quad (2)$$

where D_0 is a constant parameter, Q is the activation energy for diffusion, and R the gas constant (8.314 J mol^{-1} K^{-1}). Using the material's constants values proposed in the literature for austenitic stainless steels [13], $D_0 = 1.27 \times 10^{-6}$ m^2 s^{-1}, and $Q = 55535$/mol, the computed diffusion coefficient at 358 K is $D_{358} = 1.05 \times 10^{-14}$ m^2 s^{-1}. This diffusion coefficient was used to compute the numerical hydrogen distributions.

2.3. Fatigue testing conditions

Fatigue testing was performed using an hydraulic fatigue machine equipped with an environmental chamber that

allows to reach temperatures from room temperature (RT) up to 250 °C, testing under vacuum, nitrogen or hydrogen environments and at a maximum frequency of 5 Hz. The maximal gas pressure that can be used is 1 MPa. In this study, tests were carried out at room temperature under 0.6 MPa hydrogen pressure. A fatigue test was performed at a loading ratio $R = 0.1$ and frequency of 0.15 Hz. Fatigue pre-crack was first introduced in air, on a standard MTS fatigue machine, at a frequency of 10 Hz up to a 2.5 mm crack size. Final pre-cracking (3 mm total pre-crack) was performed under 0.6 MPa hydrogen gas pressure, and 5 Hz frequency at a constant ΔK value of 13.5 MPa $\sqrt{m}$. Fatigue crack growth test was performed under increasing ΔK conditions from 15 MPa $\sqrt{m}$ to 30 MPa $\sqrt{m}$. In this paper, the SIMS analyzed part of the specimen correspond to fatigue crack sections propagated under the final ΔK value of the test, $\Delta K = 30$ MPa $\sqrt{m}$.

2.4. SIMS analyses

The hydrogen distribution was investigated on bulk material and on fatigue crack wake (CT specimens presented in the previous section). This section presents the SIMS analyses conditions and procedures used for each specimen type.

Depth profiles were collected on sample surfaces by using a IMS 7f SIMS instrument (CAMECA, France) using a cesium $^{133}Cs^{+}$ primary ion source. For all analyses the acceleration voltage was set at 15 kV (Primary ion energy(Cs source): +10 kV, Secondary ion energy (specimen): −5 kV). The chamber pressure was 10^{-10} torr and the mass resolution $\frac{m}{\Delta m} = 600$. The hydrogen-background signal was identified on a hydrogen doped silicon substrate. For more detail on this procedure the interested reader can refer to [14]. The hydrogen backgroud signal was reduced thanks to a cold-trap. The hydrogen signal to background ratio was ranging from 10^2 to 10^3 depending on the local hydrogen content. Two type of analyses were performed. First, Element Depth Profiles (EDP) of hydrogen, iron, oxygen and carbon were performed at different locations on the specimen surface using an electron multiplier detector. When performing EDP, the surface is continuously sputtered during the analyses process so that depth profile of a given element can be evaluated. Using a dimension 3100 Veeco atomic force microscope, the total sputtered depth was evaluated to be 400 nm at the end of the analyses. In addition to EDP, secondary ion images were obtained with a resistive anode encoder (RAE) image acquisition system. In the case of RAE mapping acquisition, the analyzed area was a circular area of 100 μm in diameter.

On hydrogen charged samples, EDP were collected radially starting from the edge of the sample to the center of the specimen as shown Fig. 1. Fig. 2 illustrates a typical depth profile obtained on a charged specimen. It illustrates the high hydrogen content at the beginning of the depth profile due to unavoidable pollution traces of the surface (water molecules or organic materials attached to the specimen surface for example). However iron, hydrogen and carbon signals stabilize quickly. Only the oxygen signal exhibits unstable behavior but are not associated to carbon or hydrogen so that it does not indicate the presence of water or hydro-carbonate compounds. This unstable signal might be due to oxide inclusions or

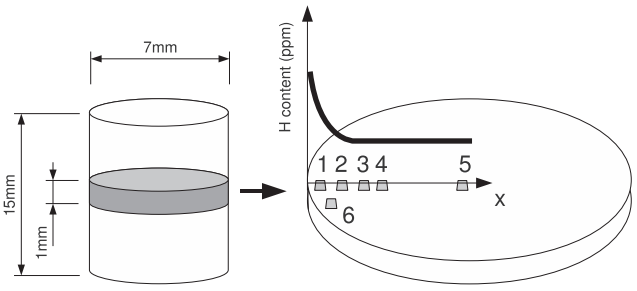

Fig. 1 – Specimen geometry for hydrogen charging and extracted specimen for hydrogen measurements by SIMS.

sulfides since the mass of $^{16}O_2$ (mass = 32) corresponds to the mass of $^{32}S^{-}$. The hydrogen signal detected here can be considered as releated to the hydrogen content in the material. In order to evaluate the hydrogen content it was assumed that:

i the hydrogen signal intensity, I_H, measured at the center of the specimen is representative of the hydrogen content in the uncharged material,
ii the iron signal, I_{Fe}, can be used to normalize the hydrogen signal for each hydrogen Depth Profile (DP).

Finally the hydrogen content was computed as follows:

$$r(x) = \frac{I_H(x)}{I_{Fe}(x)} \tag{3}$$

$$C_H(x) = \frac{r(x)}{r(x_{sc})} \times C_n(\text{in mass ppm}) \tag{4}$$

where x_{sc} is the radius of the specimen and C_n the hydrogen content inside the specimen prior to charging. Analyses were performed in series of 5 locations spaced by a distance of about 75 μm. An additional final measurement was done next to the first analysis point in order to evaluate any shift in the analysis conditions and to control that the measured hydrogen concentration gradients were not due to progressive hydrogen desorption from the surface. All results presented in

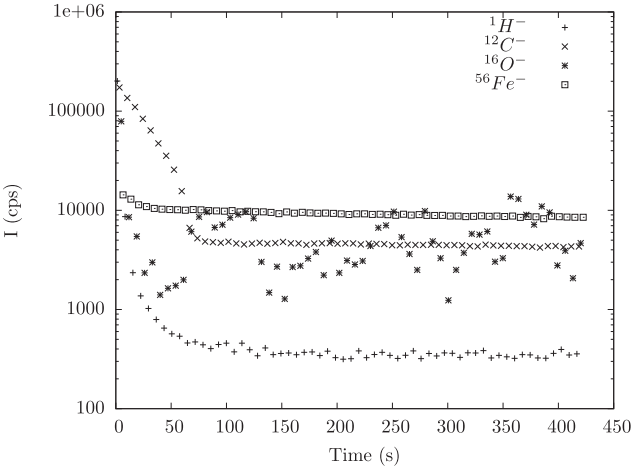

Fig. 2 – Typical evolution of the hydrogen, Carbon, Iron and Oxygen Intensity measured by SIMS on hydrogen charged specimens.

this paper correspond to analyses where the first and last measurements were found to be consistent (i.e. no variation of the hydrogen content between the beginning and the end of the analysis).

Hydrogen analyses around the fatigue crack were performed on $10 \times 10 \times 1\,mm^3$ specimens cut out from the middle plane (plane strain condition) of the CT specimen (see Fig. 3). Specimen dimensions were imposed by the SIMS holder size. They were cut so that the crack tip and crack wake regions could be investigated by SIMS. Two sets of measurements were performed. For the first set (referred as "set 1" in the rest of the paper), depth profiles were conducted perpendicularly to the crack propagation direction at 500 μm from the crack tip to preserve the crack tip region for SIMS RAE images. For "set 2" the measurements were done ahead the crack tip in the direction of the crack propagation direction.

In all cases, the experimental procedure was optimized to ensure that minor desorption was induced by the specimen preparation process as validated by previous studies in the laboratory [6].

3. Results

3.1. *H charged samples*

Fig. 4 compares the hydrogen distribution computed using equation (1) and the measured hydrogen distribution using the procedure described in the previous section. The first points very near the surface are below the predicted values from Fick's diffusion law. That may arise from both the inherent scatter of such measurments and some hydrogen egress from the specimen surface. However the experimental data set is in reasonably good agreement with the expected hydrogen distribution which validates both the specimen preparation and hydrogen content computation procedures. It is observed that significant hydrogen content was detected only in the first 200 μm from the specimen surface. Thereafter, hydrogen and iron SIMS RAE images were performed within those 200 μm and additional analyses were performed in the center of the specimen for comparison. Fig. 5 illustrates SIMS RAE images of hydrogen and iron in the case of hydrogen charged specimens. At the top left of each SIMS RAE image, a scheme indicates the location of the analyses on the specimen. In the case of SIMS RAE images, the

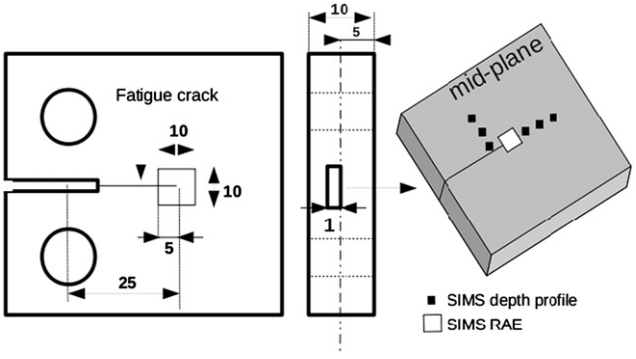

Fig. 3 – Extracted specimen from CT specimens after fatigue testing for SIMS measurement.

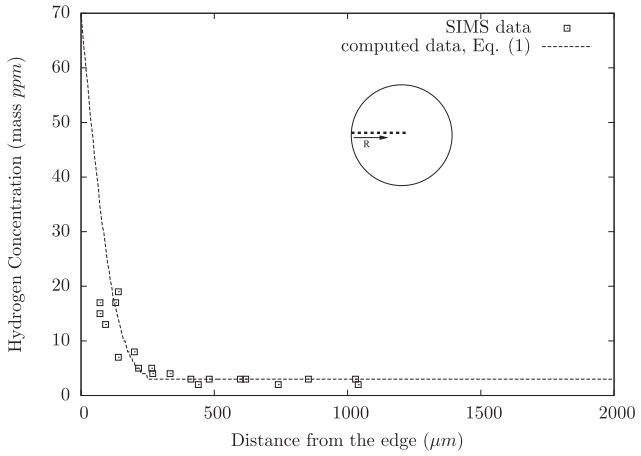

Fig. 4 – Hydrogen concentration measurements by SIMS and comparison to the computed concentrations by equation (1).

analyzed area has to be chosen so that it enables to visualize hydrogen content gradients from the surface. From the observed hydrogen distribution on depth profiles it was chosen to fix the rastering area to 150 μm × 150 μm. The analyzed area is a 100 μm diameter circle centered on the rastering area. Fig. 5(a) and (c) indicates high hydrogen content at the surface of the specimen as expected from the identified hydrogen distribution. However, the fact that the iron distribution (Fig. 5(b) and (d)) also indicates high iron content at the surface let us suppose that the observed hydrogen distribution is partially due to crater-edge effect to which SIMS RAE images are known to be sensitive. SIMS RAE images taken at 100 μm from the edge are given in Fig. 5(e) and (f). In that case the edge of the sample is not included in the raster area neither the analyzed area. No hydrogen gradient can clearly be identified but heterogeneous hydrogen distributions can be observed that can be considered as significant when compared to hydrogen distribution measured in the center of the specimen (see Fig. 5(g)). However SIMS RAE images given in Fig. 5(f) and (h) indicate heterogeneous iron distribution at the specimen surface. AFM surface analyses (see Fig. 6) of the raster area indicate that the roughness induced by the sputtering process depends on the local grain orientation. These differences in surface roughness makes quantitative analyses difficult to obtain by using RAE analyses in our context.

3.2. *Fatigue crack in CT specimen*

Fig. 7 illustrates the hydrogen distributions obtained from EDP. For the measurement "set 1", the maximum hydrogen content of about 8.5 mass ppm is located at the edge of the crack lip. The hydrogen concentration drops to the natural hydrogen concentration (2.2 mass ppm) within a millimeter. Despite some scatter in the experimental data, it is possible to identify a diffusion-like mean trend. Assuming a Fick diffusion distribution as given by equation (1), apparent diffusion parameters $C_s^\star$ and $D^\star$ were optimized so that the computed hydrogen distribution best fits the experimental data (dashed curve labeled "optimized diffusion model" on Fig. 7). The exposure time considered for the optimization process is the

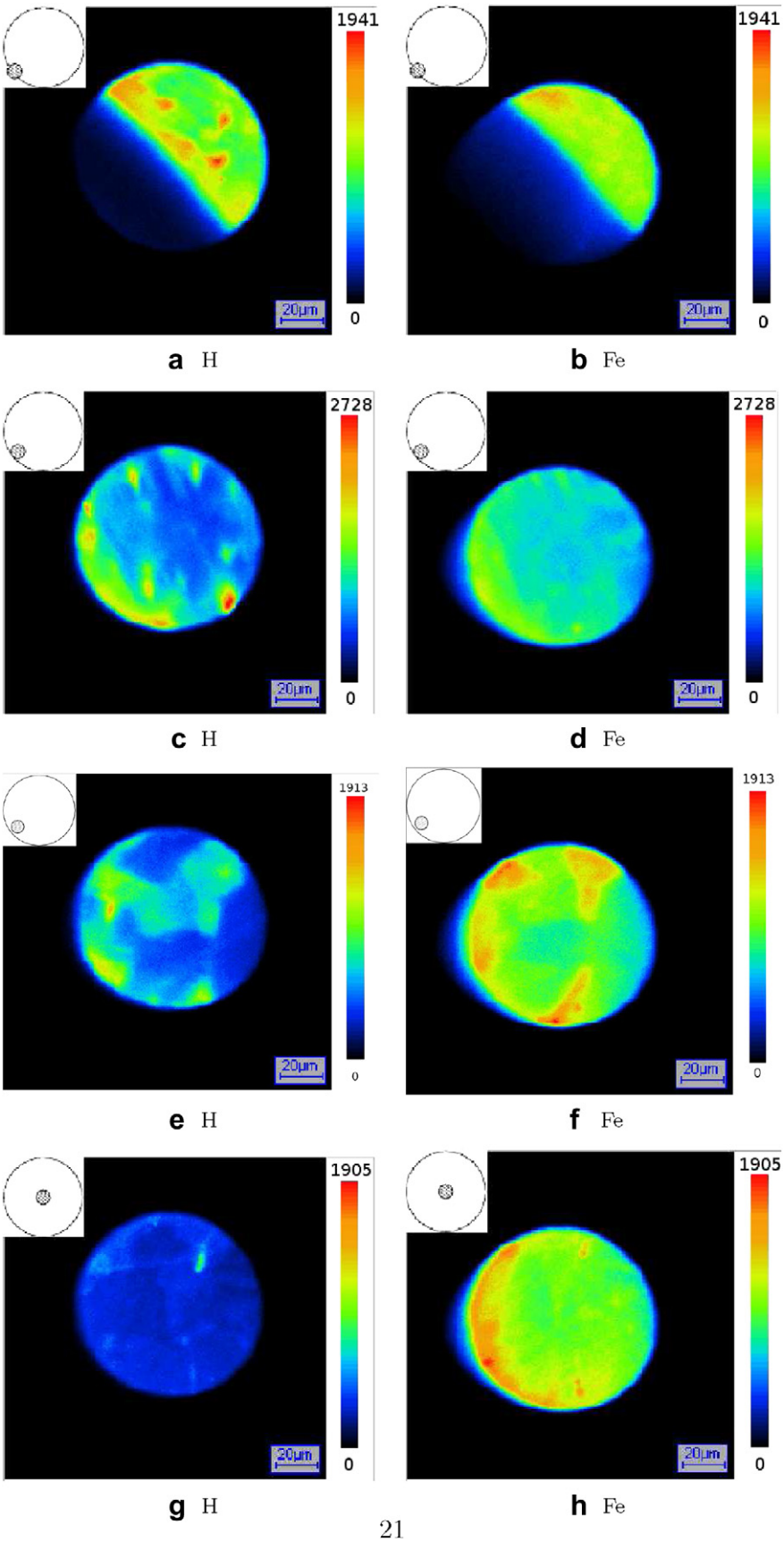

Fig. 5 – SIMS RAE images of H and Fe elements on charged samples at (a,b) the edge of the specimen, (c,d) 50 μm, (e,f) 100 μm and (g,h) 3 mm from the edge.

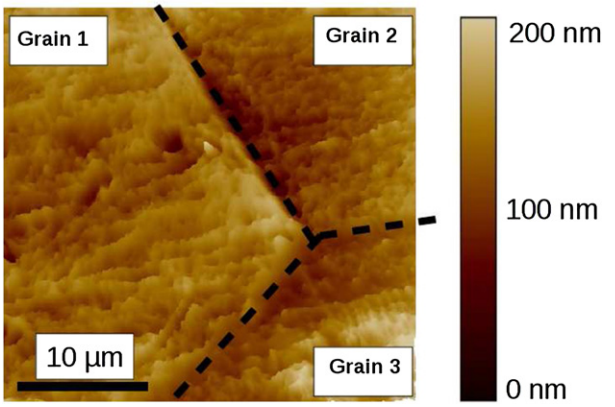

Fig. 6 – Surface topology of the raster area after the SIMS analyses. Dash lines correspond to grain boundaries.

time needed for the crack to growth from the analyses area to the final crack tip position. In our case the crack growth rate was $\frac{da}{dN} = 1.6 \times 10^{-6}$ m/cycle at $\Delta K = 30$ MPa$\sqrt{m}$ and $R = 0.1$. It has to be noticed that this exposure time has to be divided into two periods. The first one corresponds to the time needed for the active cyclic plastic zone to cross the EDP analyses area, the second one being the time of exposure to the hydrogen gas of the unloaded but highly deformed crack surface. This point will be further developed in the discussion section. The total exposure time used for the optimization is 2083 s and the apparent diffusion parameters are $C_s^\star = 6.6$ mass ppm and $D^\star = 9.0\times10^{-12}$m^{2}s^{-1}. Since the gas pressure is low (0.6 MPa) the hydrogen is considered to behave as an ideal gas and the apparent solubility $K_s^\star$ can be computed as follows :

$$K_s^\star = \frac{C_s^\star}{\sqrt{p}} \tag{5}$$

where p is the gas pressure. The value obtained is $K_s = 8.5$ (mass ppm) $\sqrt{MPa}$.

For comparison, the hydrogen distribution corresponding to pure diffusion in annealed type 304 (C_s = 3.2 mass ppm, $K_s = 4.13$ (mass ppm) $\sqrt{MPa}$ and $D = 2.7 \times 10^{-16}$m^{2}s^{-1}) is also plotted on Fig. 7 (labeled "non optimized diffusion model").

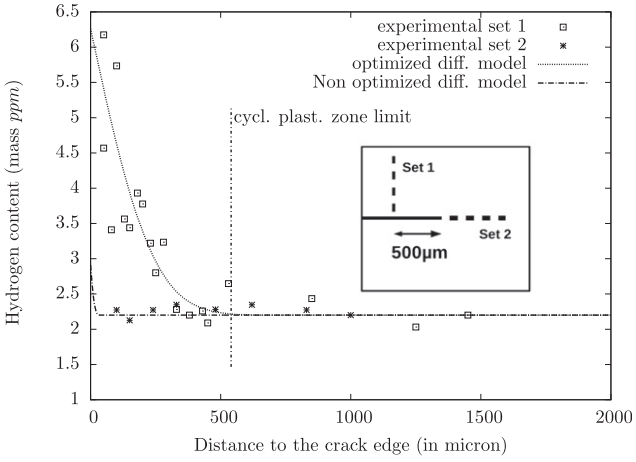

Fig. 7 – Hydrogen concentration measurements by SIMS in the crack tip region for type 304 material.

In order to relate the observed hydrogen distribution to the plastic activity the size of the plastic zone must be evaluated. In the case of fatigue cracks it is well known that two different butterfly-shaped plastic zone are developed at the crack tip : the static and cyclic plastic zones. In the case of cracks loaded in mode I, assuming small scale yielding and an elastic perfectly plastic behavior of the material, Rice [15] investigated the shape of static plastic zones. For a crack subjected to plane strain loading, the dimension of the plastic zone r_y in the direction perpendicular to the crack propagation direction (size of the crack wake) is given by:

$$r_y = 0.15\frac{K^2}{\sigma_y^2} \tag{6}$$

where K is the stress intensity factor range and σ_y the yield stress. In the case of strain hardening materials, Shih [16] proposed analytical solutions for the plastic zone contours under mixed mode I and II loading. For pure mode I loading and plane strain conditions it was shown that for strain hardening coefficient n greater than 3, the plastic zone contours were close to that of elastic perfectly plastic materials (infinite value of n). In addition, the r_y values obtained by Shih in the case of elastic perfectly plastic materials equal to the ones proposed by Rice [15]. In air, at room temperature, a typical value of $n = 5$ is reasonable for type 304 stainless steel (see for example [17]). For this reason, the r_y solution proposed by Rice will be retained in this paper. From equation (6) the cyclic plastic zone $r_{y,cl}$ will classically be computed as follows:

$$r_{y,cl} = 0.15\frac{\Delta K^2}{(2\sigma_{y,cl})^2} \tag{7}$$

Where ΔK is stress intensity factor and $\sigma_{y,cl}$ the cyclic yield stress for strain hardening or softening materials. In our case, the cyclic plasticity around the crack tip region developed in a rich hydrogen environment so that strong hydrogen–plasticity interaction occured, hydrogen being constantly provided during the deformation process. Experimental data on the effect of hydrogen on the cyclic behavior of stainless steels under such coupled hydrogen–plasticity interaction is not well documented in the literature. Also very few data are available on the mechanical behavior on homogeneously charged specimens. Murakami et al. [7], in a recent synthesis paper underlines the fact that the plastic zone sizes at the crack tip of hydrogen charged specimens can be significantly reduced compared to the ones observed on uncharged specimen. For these reasons the $r_{y,cl}$ value given by equation (7) will be considered as an upper bound of the actual cyclic plastic zone size. Considering a cyclic yield stress of 250 MPa and a ΔK value of 30 MPa $\sqrt{m}$, $r_{y,cl}$ is equal to 540 µm. For the measurement "set 2", almost no hydrogen was found ahead of the crack tip, at least after the first 100 µm.

In addition to depth profiles, SIMS RAE images were obtained at different location along the crack, the final analyses being performed on the crack wake and at the crack tip. Fig. 8(b) to (g) illustrate the results obtained on the crack wake. For all cases, the observed hydrogen distribution matches the carbon distribution. It suggests that hydrogen detected here is mostly due to

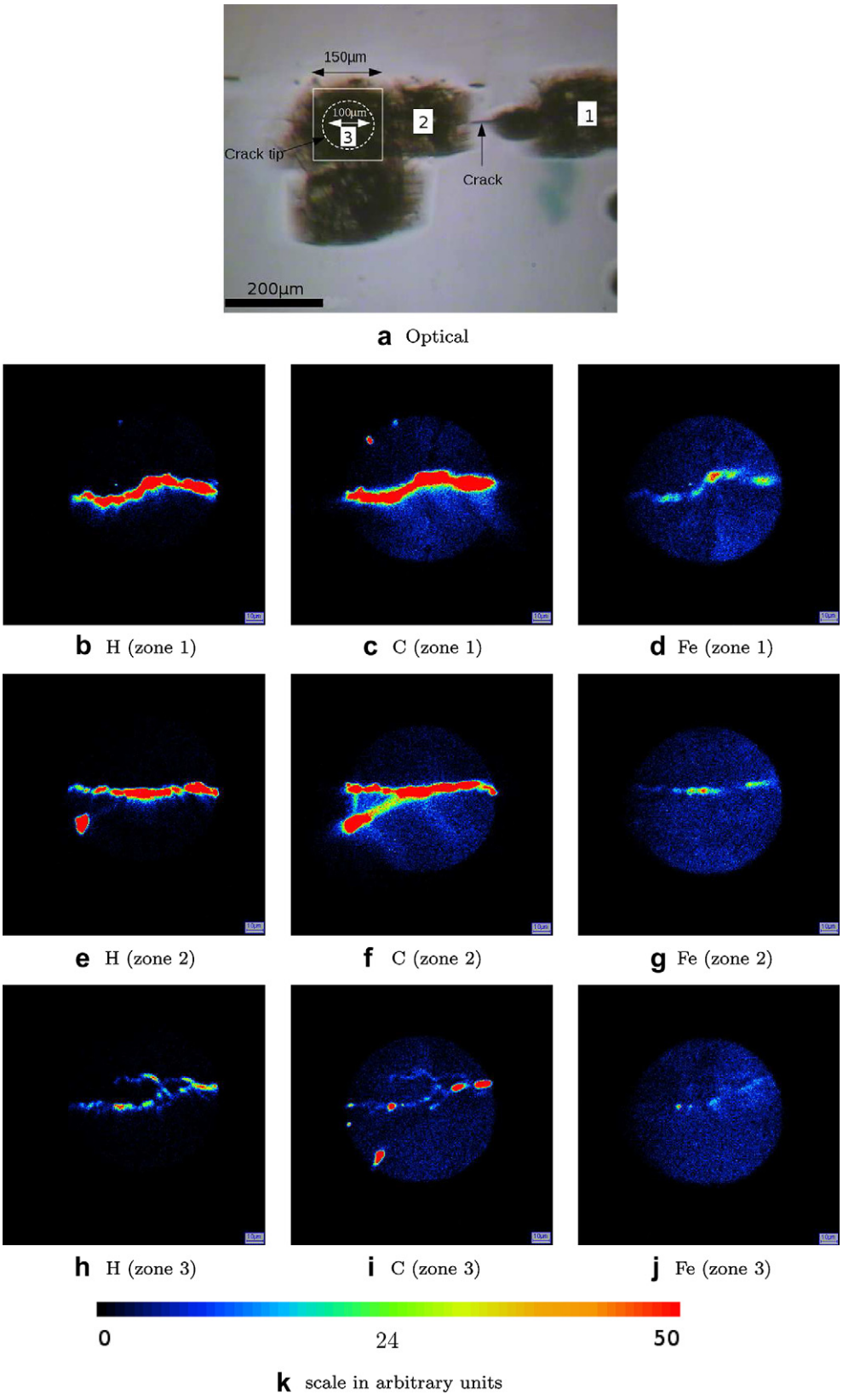

Fig. 8 – RAE of H and Fe elements on type 304 fatigue cracks, a) indicates the location of the analysed zones with respect to the crack.

pollutions that are present within the crack and that are revealed during the sputtering process. This phenomenon is increased by the fact that the crack is slightly open after testing. In that case, pollution can enter the crack during the cutting process of the small specimen out from the large CT specimen. Moreover, AFM analyses around the analyzed areas revealed heterogeneous sputtering around the crack edges and that the ion beam enters deeply into the crack. Fig. 8(h) to (j) illustrates hydrogen, carbon and iron element distribution around the crack tip region. The crack in this region is almost closed so that it limits the entry of pollution elements during the preparation process. In that case the carbon distribution is kept to a very low level. Also the iron signal is homogeneous. These are good indicators that the observed hydrogen distribution can be associated to some hydrogen in the crack tip region. However, the surface heterogeneity again prevents to make any quantitative analyses from those measurements. It was concluded that, in our context, only EDP could be used for quantitative analyses of hydrogen distribution at the crack tip.

4. Discussion

The validation of the SIMS technique to analyze atomic hydrogen content on an annealed 304 austenitic stainless steel reference specimen after exposure to high pressure hydrogen gas is shown in Section 3.1. The estimation of the hydrogen content is possible down to 2.2 mass ppm and the obtained experimental content profiles correspond to the predicted one. This result validates the analysis procedure and the use of SIMS on the crack tip and crack wake of a fatigue crack exposed to high purity hydrogen gas. In this section, the main discussion will deal with the results obtained around the fatigue crack. The data obtained by EDP analysis in the crack wake (set 1) of the fatigue crack allowed us to estimate by optimization an apparent diffusion coefficient D^*. This coefficient D^* ($D^\star = 9.0 \times 10^{-12} m^2 s^{-1}$) is five orders of magnitude higher than the diffusion coefficient obtained on annealed FCC material at the same temperature ($D = 2.7 \times 10^{-16} m^2 s^{-1}$, eq. (2) and material parameters from [13]). This high difference is ten times higher the well established one existing between the diffusivities of austenite and strain-induced martensite at room temperature. In addition, the apparent hydrogen solubility $K_s^\star$ obtained from the measurements is twice the hydrogen solubility K_s of annealed material.

As described in the results Section 3.2, the exposure time to hydrogen gas of the crack wake zone analyzed by EDP can be expressed as the sum of two periods: namely, the period t_c for the cyclic plastic zone to cross the zone of analysis, and t_e the exposure time of the crack wake analyzed zone to the hydrogen gas. The period t_c is obtained by:

$$t_c = \frac{r_x}{f}\left(\frac{da}{dN}\right)^{-1} \quad (8)$$

with $r_x = 0.036\Delta K^2/\sigma_y^2$ [15], the cyclic plastic zone size ahead the crack tip equals to 129 μm in our case, $f = 0.15$ Hz and $\frac{da}{dN} = 1.6 \times 10^{-6} m/cycle$. The value of t_c is about 537 s. The hydrogen diffusion during this period is probably very high due to the slip-off process existing in the cyclic plastic zone region. The second period, t_e, is defined by a similar approach but considering the distance between the analysis zone and the final crack tip position that is 500 μm instead of r_x, the obtained value is $t_e = 2083$ s. During this period pure diffusion is acting. The apparent $D^\star$ coefficient is then a combination of a cyclic plasticity driven diffusion (probably diffusion and transport by dislocations) $D_c^\star$ and of a pure diffusion $D_e^\star$ in a highly cyclically deformed material.

For pre-strained type 304, 316L and 310S stainless steels, Mine et al. [18] investigated the effect of cold-working (pre-straining) on the hydrogen solubility and diffusivities. For 304 type stainless steel and pre-strain (ϵ_{pre}) ranging from 0 to −0.92, hydrogen solubility was found to be rather stable, whereas the hydrogen diffusivity at $\epsilon_{pre} = -0.92$ was one decade above the one measured on not pre-strained material ($\epsilon_{pre} = 0$). It must be noted that in that case the pre-straining induces strong phase transformation (from 18% to 39% of strain-induced martensite depending on the pre-straining value). Under similar charging and pre-straining conditions, on 316L (fcc phase), the diffusivity was only slightly modified while the solubility K_s was 35% higher in pre-strained ($\epsilon_{pre} = -0.92$) material compared to undeformed material. Similar trend was observed on type 310S. For type 316L and type 310S, due to their stability, no martensitic phase transformation was induced by monotonic plastic deformation. In our case, EBSD analyses on the crack wake (see Fig. 9) reveal that under those particular mechanical and environmental conditions, the martensitic phase transformation zone was discontinuous and of a few micron (<5 μm) in size (those observations are consistent with the one given by Kanezaki et al. [19]). From those observations it can be considered that the hydrogen enrichment in the first 500 μm is not due to the presence of strain-induced martensite that is known to exhibit higher diffusivity coefficient compared to austenite but most probably to the cyclic plastic deformation at the crack tip. In the following, we will then consider that thehydrogen diffuses in a deformed austenite phase. From the previously cited results obtained by Mine et al on stable autenitic stainless steels, it was shown that the diffusion coefficient is not strongly modified by plastic pre-straining so that $D_e^\star$ can be considered as close to the one measured on undeformed austenite so that $D_c^\star \approx D^\star$. It can be concluded that the observed hydrogen distribution results from a strong coupling between the localized cyclic plasticity acting at the crack tip and the hydrogen diffusion process. As shown Fig. 7, the hydrogen distribution drops to the natural hydrogen content (2.2 mass ppm) at a distance from the crack tip that is close to the computed plastic zone size. This supports the hypothesis of an active hydrogen transport by dislocations during the deformation process.

The hydrogen solubility increase is significant (twice the one of undeformed material) compared to the solubility increase measured on pre-strained material (1.3 times the one of undeformed material [18]). The hydrogen solubility is directly linked to the trapping site density. The dislocation density and dislocation structures after completion of the deformation process at the crack tip differ significantly from the one resulting from monotonic pre-straining [20,21]

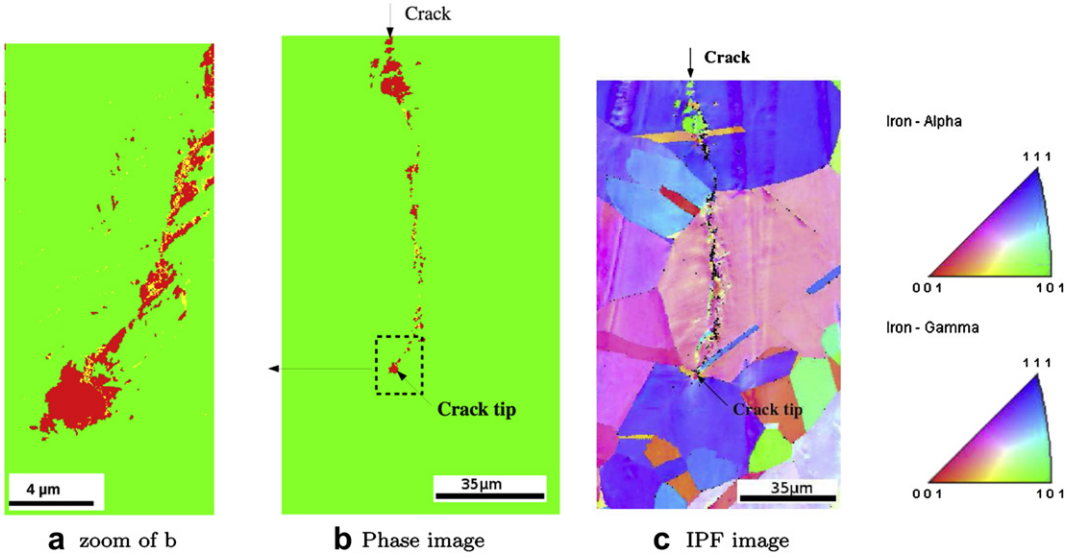

Fig. 9 – EBSD analyses of the crack tip region. a) Phase image (BCC (red), FCC (green), not indexed (yellow)) and b) corresponding Inverse Pole Figure (f = 0.15 Hz, ΔK=30 MPa$\sqrt{m}$, P_H = 0.6 MPa). (For interpretation of the references to colour in this figure legend, the reader is referred to the web version of this article.)

resulting in a much higher trapping site density for the fatigue crack configuration.

The effect of plastic deformation on hydrogen transport hydrogen has been studied for decades but the data are relatively scares compared to the ones concerning the hydrogen embrittlement issue. Different techniques of hydrogen content measurements as well as hydrogen charging techniques have been used leading more or less to hydrogen-induced phase transformation and hydrides or deuteride formation depending both on the external hydrogen activity applied and on the microstructural stability of the materials. Brass et al. [22] proposed a review of experimental data on the influence of deformation on hydrogen behavior in iron and nickel base alloys. Asserting that in all experimental conditions the transport of hydrogen by the dislocations exists would be abusive since opposite evidences can be found in the literature. It must be noted that the data available in the literature on the transport of hydrogen by the dislocations were all obtained under monotonic mechanical loading and not under fatigue conditions. Ladna et al. [23] were the first to study the possible effect of hydrogen transport during plastic deformation using SIMS in type 304 and 310 stainless steels and in nickel. Cathodic polarization at room temperature in 1N D_2SO_4 containing 0.25 g l^{-1} $NaAs_2O_3$, was applied (20 mA cm^{-2}) to specimens during straining at 8.5 × 10^{-5} s^{-1} and to other specimen without mechanical loading. From the analysis of in depth deuterium (D) content profiles, the authors observed no effect of plasticity on deuterium uptake in 310. On 304 the modification of the D content profiles obtained during straining was attributed to the strain-induced martensitic transformation. In the case of nickel, the D charging conditions have always led to the formation of hydrides and the authors explained the shift of the D content profiles by the effect of the hydride layer brittle fracture. From all these results, the authors concluded an absence of significant contribution of dislocation transport to the D diffusion.

One of the key points evoked by the author is the absence of a net flux of dislocations from the surface to the bulk of the specimen: during straining of a poly-crystalline specimen the external hydrogen produced at the surface cannot be transported to the bulk by the dislocations. The fact that such a net flux does exist in the case of single crystal may explain some different experimental results. Other conclusions were obtained in more recent experimental studies by applying different techniques. Using β counting of tritium desorption during monotonic plastic deformation in 316L steel, for the temperature and strain rate conditions considered (20 C, 2.0 × 10^{-4}–2.0 × 10^{-5} s^{-1}), evidences of hydrogen dragging by strain-induced mobile dislocations supported a role of dislocation transport. To avoid hydrogen-induced phase transformations, electrochemical charging conditions were carefully chosen by Brass et al. [24], and especially no recombination poisons were used. On 316L and for high external hydrogen activity (cathodic polarization during straining at room temperature in 1N H_2SO_4 and 0.25 g l^{-1} As_2O_3, 100 mA cm^{-2}), slow strain rate tests for strain rates ranging between 7.0 × 10^{-7} and 5.0 × 10^{-6} s^{-1} were performed. Based on the observed decrease of the strain to fracture, Herms et al. [25] have shown that hydrogen transport by dislocations from the surface to the bulk of the material was operating at a propagating crack tip. Quantitative data on the dragging mechanism of hydrogen by dislocations were obtained by Chene et al. on nickel-based superalloy single crystals oriented for easy glide. Strong evidence for hydrogen accelerated transport by dislocations was shown. Tritium desorption from tritiated samples undergoing tensile straining allowed the authors to roughly estimate an upper bound of the normalized number of hydrogen atoms transported by dislocation was 50 atom/b (b, the burger vector) [26]. Hydrogen transport by dislocation in alloy 600 was shown by the same author by studying strain-assisted desorption of tritium [27]. Permeation tests simultaneous performed with slow strain

rate test on AISI 4120 steel and bainitic 2.25Cr-1Mo and 3Cr–1Mo–V steels have shown a strong contribution of an enhanced transport of hydrogen by mobile dislocations. These results obtained by Brass et al. were based on the strain-rate effect analysis [28]. More recent data where obtained on pure Iron and Inconel 625 by Shoda et al. [29]. Analysis of hydrogen desorption behavior during tensile deformation were performed in situ by using slow strain rate testing of hydrogen charged specimens placed in a vacuum chamber connected to a quadrupole mass spectrometer. Based on the analysis of the strain rate dependence of hydrogen desorption, the authors could show clearly the hydrogen transport by dislocations for the two bcc and fcc materials studied. From all these results, it is clear that different experimental approaches (internal or external hydrogen, hydrogen activity level, poly or single crystals) can lead to different conclusions. In the present study, the fatigue crack growth process is the slip-off one (see for exemple Oda [30]). Indeed, the applied gaseous hydrogen conditions correspond to low hydrogen activity and no change of propagation mode from ductile fatigue to quasi-cleavage or intergranular modes are observed. The slip-off process at the growing crack tip consists of successive movements of new dislocations at each cycle producing a net flux of dislocations from the bare surface at the crack tip to the bulk of the so-called cyclic plastic zone. As said in the results Section, almost no hydrogen was found from 100 μm ahead of the crack tip. Fig. 10 illustrates the outer surface of the specimen after testing. The darkened area corresponds to the area where intense slip activity can be found. AFM observations confirmed that only few slip bands could be found ahead of the crack tip and that they mostly developed in a marked butterfly like area. In other words, regions of low hydrogen content correspond to areas of low plastic activity (few plastic slip traces ahead the crack tip in the crack propagation direction) while high hydrogen content regions (perpendicularlly to the crack propagation direction) correspond to highly cyclically deformed areas. That result supports the idea of an active hydrogen transport by dislocations during the deformation process.

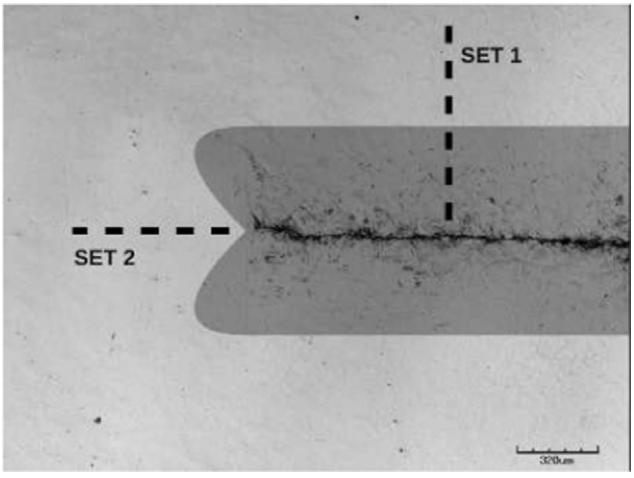

Fig. 10 – Laser microscope image of the crack tip at the surface of the specimen. The dark grey area indicates the zone of intense plastic slip bands formation (f = 0.15 Hz, ΔK=30 MPa$\sqrt{m}$, P_H = 0.6 MPa).

The approach proposed by Kotake et al. [31], based on the pionner work of Krom [32] and Sofronis [33,34], in the case of cyclically loaded cracks in an hydrogen environment have shown that the diffusion was driven by the hydrostatic stress state gradients (lattice site diffusion) and plastic strain rate (trapping site diffusion). However several points make impossible the direct use of such data in our context. First the material parameters describing the trap site density function of the plastic strain are the one of impure iron used by Sofronis and McMeeking [35]. Those parameters may not be adequate for stainless steels since the dislocation density to plastic strain relation are quite different. Secondly, the diffusivity coefficients and characteristic loading time are quite different to the one of the present study. And finally, the hydrogen distributions are analyzed in the crack propagation direction whereas we analyzed in the perpendicular direction to the crack tip. Future work will focus on coupled plasticity-diffusion models in the case of cyclically loaded cracks for stainless steels in order to further understand the observed hydrogen distribution.

5. Conclusion

SIMS analyses were carried out ex situ on type 304 austenitic stainless steel exposed to hydrogen gas under two conditions, namely: exposure to 10 MPa hydrogen gas of annealed specimen; exposure to 0.6 MPa hydrogen gas of CT specimen during fatigue crack propagation. From the obtained data, the following conclusions can be proposed:

- On annealed specimen exposed to high pressure hydrogen, EDP SIMS mode is able to describe quantitatively the hydrogen profile content. It is more difficult to obtain such results by using the RAE mode mainly because of a larger hydrogen-background (low sputtering rate due to the larger raster size in the mapping).
- Based on the hydrogen content profile measured by EDP in the fatigue crack wake, an apparent diffusivity four order of magnitude higher than the one on annealed material is estimated. This high diffusivity is proposed to result from the cyclic plastic activity at the crack tip, the mechanism of propagation being the slip-off one. The distance from the fatigue crack tip in which hydrogen content is significantly higher than the native content is about 180 times higher than the distance computed using the diffusivity of annealed or even the one obtained on pre-strained material. This result is consistent with the more localized slip band found in the plastic zone relatively far from the fatigue crack.
- The apparent solubility obtained is this study is 8.5 mass ppm $\sqrt{MPa}$, that is about twice the one observed on fcc stable phase (type 316L) pre-strain at −0.92 by cold-working. This result is linked to the dislocation dynamics, density and structure specific to the fatigue crack tip zone leading to a strong effect on hydrogen transport.

The results presented here show clearly the necessity to use the SIMS technique around fatigue crack tip exposed to

hydrogen gas for a quantitative estimate of hydrogen content. SIMS allows to analyze hydrogen–plasticity interaction in a highly coupled configuration that cannot be accessed by usual global hydrogen content measurement methods. Also, it allows to identify (or optimize) hydrogen diffusion parameters used in numerical simulations that may only partially be identified from experimental data on less coupled configuration such as analysis of pre-strained material (monotonically or cyclically). For understanding the strong effect of the frequency on fatigue crack growth rate in material exposed to hydrogen gas, it will be crucial to use the SIMS technique under EDP mode as it was done in this study. Further work has to be done to improve the RAE mode in this context.

Acknowledgement

This research was supported by the NEDO project "Fundamental Research Project on Advanced hydrogen science" (2006–2012). The authors, N. Saintier and J.M. Olive are grateful to NEDO, Arts et Métiers ParisTech and CNRS for their financial support during their stay at Kyushu University.

REFERENCES

[1] Murakami Y, Matsunaga H. Effects of hydrogen on fatigue crack growth behavior of austenitic stainless steels. Int J Fatigue 2008;28(10):1509–20.
[2] Barthelemy H. Effects of pressure and purity on the hydrogen embrittlement of steels. Int J Hydrogen Energy 2011;36:2750–8.
[3] Vennett R, Ansell G. The effect of high-pressure hydrogen upon the tensile properties and fracture behavior of 304l stainless steel. Trans Am Soc Met 1967;60:242–51.
[4] Benson JR, Dann R, Roberts JL. Hydrogen embrittlement of stainless steel. Trans Metall Soc AIME 1968;242(10):2199–205.
[5] Birnbaum H, Sofronis P. Hydrogen-enhanced localized plasticity-a mechanism for hydrogen related-fracture. Mater Sci Eng A 1994;176:191–202.
[6] Murakami Y, Kanezaki T, Mine Y, Matsuoka S. Hydrogen embrittlement mechanism in fatigue of austenitic stainless steels. Metallurgical Mater Trans A 2008;39(6):1327–39.
[7] Murakami Y, Matsuoka S. Effect of hydrogen on fatigue crack growth of metals. Engng Fract Mech 2010;77(11):1926–40.
[8] Kanezaki T, Narazaki C, Mine Y, Matsuoka S, Murakami Y. Effects of hydrogen on fatigue crack growth behavior of austenitic stainless steels. Int J Hydrogen Energy 2008;33(10):2604–19.
[9] Mine Y, Narazaki C, Kanezaki T, Matsuoka S, Murakami Y, Fatigue behaviour of metallic materials exposed to high pressure hydrogen environments. In: Proceedings of the 16th European Conference of Fracture (ECF16) CD-ROM.
[10] Takai K, Chiba Y, Noguchi K, Nozue A. Visualization of the hydrogen desorption process from ferrite, pearlite, and graphite by secondary ion mass spectrometry. Metall Mater Trans A 2002;33:2659–65.
[11] Brass AM, Chene J, Boutry-Forveille A. Measurements of deuterium and tritium concentration enhancement at the crack tip of high strength steels. Corr Sci 1996;38(4):569–85.
[12] Chene J, Lecoester F, Brass AM, Noel D. Sims analysis of deuterium diffusion in alloy 600: the correlation between fracture mode and deuterium concentration profile. Corr Sci 1998;40(1):49–60.
[13] Mine Y, Horita Z, Murakami Y. Effect of hydrogen on martensite formation in austenitic stainless steels in high-pressure torsion. Acta Mater 2009;57(10):2993–3002.
[14] Miwa S, Nomachi I, Kitajima H. High sensitivity analysis of atmospheric gas elements. Appl Surf Sci 2006;252:7247–51.
[15] Levy N, Marcal P, Ostegren W, Rice J. Small scale yielding near a crack in plane strain: a finite element analysis. Int J Fracture Mech 1971;7:143–56.
[16] Shih CF. Small-scale yielding analysis of mixed mode plane strain crack problems. ASTM STP 1971;560:187–210.
[17] Xue H, Shi Y. Ctod design curve in consideration of material strain hardening. Int J Press Vessels Piping 1998;75(7):567–73.
[18] Mine Y, Narazaki C, Murakami K, Matsuoka S, Murakami Y. Hydrogen transport in solution-treated and pre-strained austenitic stainless steels and its role in hydrogen-enhanced fatigue crack growth. Int J Hydrogen Energy 2009;34(2):1097–107.
[19] Kanezaki T, Mine Y, Matsuoka S, Murakami Y. Hydrogen induced fatigue crack growth acceleration and martensitic transformation of austenitic stainless steels. In: Proceedings: International Hydrogen conference, effect of hydrogen on materials. Wyoming, USA: Jakson Lake lodge; 2008.
[20] Feaugas X, Gaudin C. Different levels of plastic strain incompatibility during cyclic loading: in terms of dislocation density and distribution. Mat Sci Engng A 2001;309–310:382–5.
[21] Feaugas X, Haddou H. Effects of grain size on dislocation organization and internal stresses developed under tensile loading in fcc metals. Phil Mag 2007;87(7):989–1018.
[22] Brass AM, Chene J. Influence of deformation on the hydrogen behavior in iron and nickel base alloys: a review of experimental data. Mater Sci Eng A 1998;242(1–2):210–21.
[23] Ladna B, Birnbaum H. A study of hydrogen transport during plastic deformation. Acta Metal 1987;35:1775–8.
[24] Brass A, Chene J. Hydrogen uptake in 316l stainless steel: consequences on the tensile properties. Corros Sci 2006;48:3222–42.
[25] Herms E, Olive JM, Puiggali M. Hydrogen embrittlement of 316l type stainless steel. Mater Sci Eng A 1999;272(2):279–83.
[26] Chene AMBJ. Hydrogen transport by mobile dislocations in nickel base superalloy single crystals. Scripta Materialia 1999;40:537–42.
[27] Chene J. Strain-assisted transport of hydrogen and related effects on the intergraular stress corrosion cracking of alloy 600. Environment-Induced Cracking Mater; 2008:261–72.
[28] Brass A-M, Chene J. Influence of tensile straining on the permeation of hydrogen in low alloy cr-mo steels. Corros Sci 2006;48:481–97.
[29] Shoda H, Suzuki H, Takai K, Hagihara Y. Hydrogen desorption behavior of pure iron and inconel 625 during elastic and plastic deformation. ISIJ Int 2010;50:115–23.
[30] Oda Y, Furuya Y, Noguchi H, Higashida K. Afm and sem observation on mechanism of fatigue crack growth in a fe-si single crystal. Int J Fract 2002;113:213–31.
[31] Kotake H, Matsumoto R, Taketomi S, Miyazaki N. Transient hydrogen diffusion analyses coupled with crack-tip plasticity under cyclic loading. Int J Press Vessels Piping 2008;85(8):540–9.
[32] Krom AHM, Koers RWJ, Bakker A. Hydrogen transport near a blunting crack tip. J Mechanics Phys Solids 1999;47(4):971–92.
[33] Taha A, Sofronis P. A micromechanics approach to the study of hydrogen transport and embrittlement. Engng Fract Mech 2001;68(6):803–37.
[34] Kanayama H, Ogino M, Miresmaeili R, Nakagawa T, Toda T. Hydrogen transport in a coupled elastoplastic-diffusion analysis near ablunting crack tip. J Comp Sci Tech 2008;2(4):499–510.
[35] Sofronis P, McMeeking R. Numerical analysis of hydrogen transport near a blunting crack tip. J Mech phys Solids 1989;37(3):317–50.